The near-field scanning thermal microscope

Uli F. Wischnath,[a] Joachim Welker, Marco Munzel, and Achim Kittel[b]
Institut für Physik, Carl von Ossietzky Universität, D-26111 Oldenburg, Germany

(Received 7 March 2008; accepted 16 June 2008; published online 23 July 2008)

We report on the design, characterization, and performance of a near-field scanning thermal microscope capable to detect thermal heat currents mediated by evanescent thermal electromagnetic fields close to the surface of a sample. The instrument operates in ultrahigh vacuum and retains its scanning tunneling microscope functionality, so that its miniature, micropipette-based thermocouple sensor can be positioned with high accuracy. Heat currents on the order of 10^{-7} W are registered in z spectroscopy at distances from the sample ranging from 1 to about 30 nm. In addition, the device provides detailed thermographic images of a sample's surface. © *2008 American Institute of Physics.* [DOI: 10.1063/1.2955764]

I. INTRODUCTION

Scanning thermal microscopy (SThM) by now is an established technique for imaging the temperature distribution on surfaces of nanostructured materials, with a spatial resolution reaching the sub-500-nm scale.[1] Typical SThM devices operate under ambient conditions, implying that the heat transfer between the sample and the tip of the respective thermal profiler is mediated by gas molecules, by a liquid film of adsorbates, or even the solid-solid conduction. In contrast, the instrument described in this paper utilizes a quite different mechanism of heat transfer, namely, near-field heat radiation associated with evanescent modes of the thermal electromagnetic field. The thermal electromagnetic fields within a body are caused by charge fluctuations and consist of a wide spectrum of frequencies and k vectors. When these fields encounter the surface they are either transformed to propagating thermal radiation or they are reflected back into the body, depending on the magnitude of the k component parallel to the surface. However, in analogy to the tunneling effect for electrons the reflected fields extend into the vacuum. These decaying parts are the evanescent electromagnetic field which can only be detected close to the surface of a sample. This mechanism is much weaker than ordinary heat conduction through molecules of a gas or liquid, and thus negligible under ambient conditions. However, unlike ordinary conduction this mechanism also prevails in vacuum. In a scanning tunneling microscope (STM) based setup there is no phononic contact between the solids and therefore the evanescent fields become the only mechanism of heat transfer.

Our effort to develop a near-field SThM (NSThM) operating in ultrahigh vacuum (UHV) and detecting precisely the heat transfer proceeding via evanescent modes is spurred by the fact that such near-field radiation gives detailed information about the dielectric properties of the sample. Rytov *et al.* were the first to study such phenomena from the theoretical point of view.[2,3] Pioneering measurements of near-field heat transfer between two optically flat chromium plates have been performed by Hargreaves.[4] While his experiments gave a clear indication of the effect, they had to remain restricted to plate distances of some 100 nm. Subsequently, Polder and Van Hove gave a detailed theoretical analysis of the radiative heat transfer between two closely spaced bodies with parallel surfaces, emphasizing the complex manner in which the heat transfer depends on the dielectric functions of the materials involved.[5]

It was only after the invention of scanning probe techniques[6–8] that it became possible to perform measurements of near-field heat transfer at distances on the order of 10 nm or less. An early attempt gave no positive result; instead, from the absence of a signal an upper limit for the magnitude of the near-field heat current across a vacuum gap was deduced.[9,10] The first clear evidence of radiative near-field heat transfer in an UHV SThM was obtained with a prototype of the instrument described here.[11,12] Quite recently, a thermal radiation STM has been introduced. That device employs an oscillating tip for scattering components of the thermal near field to a remote detector;[13] it was able to detect spatial coherence effects in near-field thermal emission. Our NSThM works in a complementary manner: the thermal near field is coupled into the tip. It is operated directly at the sample's surface, i.e., at distances ranging from about 1 to some 10 nm. The data given in this paper are all obtained with a gold-coated platinum wire above a gold surface. In principle, all materials which are sufficiently conductive to allow for a tunneling current can be used as samples, and all kinds of thermocouples that can be realized sufficiently small can be used as probes. Our instrument is capable of recording the dependence of near-field radiative heat transfer on the distance between sample and probe, and of imaging the thermal near-field residing at a sample's surface.

This paper is organized as follows: Sec. II provides a general description of the instrument, together with an explanation of its working principle. A key feature of our setup are submicron micropipette-based thermocouple sensors, the manufacturing of which is outlined in Sec. III. In Sec. IV we

[a]Electronic mail: u.wischnath@uni-oldenburg.de.
[b]Electronic mail: kittel@uni-oldenburg.de.

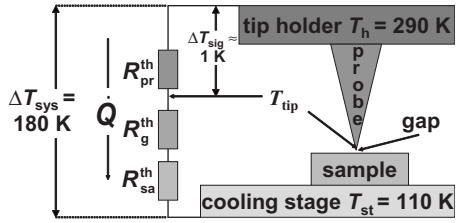

FIG. 1. Heat flow in the NSThM (schematically). The tip holder, kept at ambient temperature T_h=290 K, serves as source for the heat flow $\dot{Q}$. This flow passes through the probe, the vacuum gap, and the sample, and finally reaches the sink provided by the cooling stage at temperature T_{st}=110 K. The total temperature difference thus is ΔT_{sys}=180 K. The measured thermovoltage is due to the much smaller temperature difference $\Delta T_{sig}=T_h-T_{tip}$ between the tip holder and the very end of the tip.

then describe how such probes can be characterized with respect to both their electrical and their thermal properties. Section V discusses results of measurements made with the NSThM, from which conclusions are drawn in Sec. VI.

II. GENERAL DESCRIPTION OF THE SETUP

Our near-field SThM is based on a modified commercial UHV variable temperature STM. The microscope tip is a submicron gold-platinum thermocouple which, on the one hand, provides a thermovoltage from which the near-field-mediated heat current flowing through the gap between the probe's tip and the sample can be deduced, while retaining the STM functionality on the other, so that the STM mode can be used for precisely positioning the probe in all three dimensions. The system is operated at pressures of 10^{-8} Pa (10^{-10} mbar), which ensures that parasitic heat transfer via adsorbates or gas molecules is negligible. The sample temperature can be controlled with a cooling stage connected to a liquid-helium cryostat, allowing for sample temperatures down to 40 K. In the present experiments liquid nitrogen is used, resulting in a lower limit of the temperature of T_{sa} =110 K.

The thermovoltage signal is caused by a temperature difference ΔT_{sig} between the tip holder, which serves as a thermal bath at room temperature T_h=290 K for the probe, and the very end of the probe's tip, which cools down slightly because of radiative heat transfer to the closely spaced cold sample. As depicted in Fig. 1, in dynamic equilibrium there is a constant heat flow $\dot{Q}$ from the tip holder to the cooling stage, passing through the probe, the vacuum gap, and the sample, driven by the overall temperature difference $\Delta T_{sys}=T_h-T_{st}$ between tip holder and cooling stage. Denoting the thermal resistance of the probe by R^{th}_{Pr}, that of the gap by R^{th}_g, and considering that the thermal resistance of the sample is negligible, the equality of the heat current through each section implies

$$\dot{Q}=\frac{\Delta T_{sys}}{R^{th}_{Pr}+R^{th}_g}=\frac{\Delta T_{sig}}{R^{th}_{Pr}}, \tag{1}$$

giving

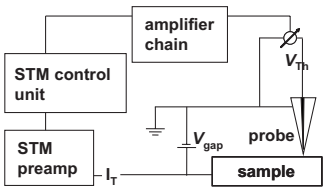

FIG. 2. Electrical setup of the NSThM. The STM gap voltage is applied to the sample, while the outer gold film of the probe is connected to ground. The thermovoltage is measured between the inner platinum wire and ground. Fluctuations of the gap voltage then do not cause noise on the thermovoltage signal.

$$\Delta T_{sig}=\frac{R^{th}_{Pr}}{R^{th}_{Pr}+R^{th}_g}\Delta T_{sys}. \tag{2}$$

This shows that sufficiently high ratios R^{th}_{Pr}/R^{th}_g are required for obtaining a temperature difference ΔT_{sig} capable of producing a significant thermovoltage V^{th}. Since the latter two quantities are linearly related through the equation

$$V^{th}=S\Delta T_{sig}, \tag{3}$$

with the probe's Seebeck coefficient S as proportionality constant, one has

$$\dot{Q}=\frac{V^{th}}{SR^{th}_{Pr}}. \tag{4}$$

Thus, the quantity of interest, the heat current $\dot{Q}$, can be determined from the measured thermovoltage signal V^{th} if both S and R^{th}_{Pr} are known.

The electrical setup of the STM had to be changed in order to enable simultaneous measurements of the thermovoltage and the tunneling current. In the original STM the gap voltage was applied to the probe, whereas the sample had been connected to ground. In this configuration, fluctuations of the gap voltage would significantly influence the thermovoltage signal connected in series. In our instrument, therefore, the gap voltage is applied to the sample, while the probe's outer gold film is grounded. The thermovoltage is then measured between the inner platinum wire and ground, as sketched in Fig. 2. The signal is fed into the control unit of the STM to acquire the data simultaneously at each individual position together with the height information of the STM.

III. MANUFACTURING OF THE PROBE

The submicron thermocouple sensor constitutes a key element of the NSThM. Such a probe should satisfy several requirements: it should be as small as possible, in order to restrict its interaction with the thermal electromagnetic field to as small a volume as possible, thus allowing measurements of the field in the immediate vicinity of the sample with high spatial resolution. In addition, it must serve as an ordinary STM tip. Finally, according to Eq. (2) its thermal resistance has to be high enough to ensure a sufficient temperature difference ΔT_{sig} between the tip and the holder.

Previously realized small thermocouple probes have been fabricated, for example, by coating a sharp-ended metal wire with a liquid insulator, which is dried. Because of the surface tension the liquid cannot cover the sharp tip, i.e., this

procedure leaves the tip uncovered, and further coating with a second metal film results in thermocouples with active regions possessing linear extensions of about 1 μm.[14,15] Other approaches include fabrication by means of electron-beam lithography, micromachining of silicon, or utilizing high electric fields at tips.[16,17]

The coaxial thermocouple making up the probe of our NSThM uses glass as the insulator between an inner platinum wire and an outer gold layer.[18] It is made from a borosilicate pipette (outer diameter of 1.25 mm, inner diameter of 0.31 mm), into which a 25 μm platinum wire is introduced. The pipette with the wire inside is then processed further in a micropipette puller, in order to realize a sharp tip with the wire protruding from a tight glass mantle. Forming the two materials jointly in the micropipette puller is only possible if the ratio of the outer diameter of the glass capillary to that of the platinum wire falls into a certain range.[18] In a first processing step a suitable ratio is reached by reducing the glass diameter through pulling. The second step, consisting of three heating periods during which the position of the pipette is kept fixed and the glass is molten, serves to achieve a tight glass covering around the wire. The third step then consists of several substeps, during which the glass/wire system is gradually stretched until a diameter of about 80 μm is reached. Finally the pipette is heated more vigorously while pulling; the tip forms when the glass pipette eventually breaks.

Good tips have at their front end a glass diameter of less than 2 μm with a platinum wire having a diameter of a few 100 nm protruding approximately 500 nm. The radii of their metal tips at the wires' very end are smaller than 50 nm as deduced from scanning electron microscope (SEM) images. The glass pipette is then fixed with a nonconducting epoxy resin in a tip holder, and coated with a 2 nm chromium layer which improves the adhesion of the 20-nm-thick outer gold film. A SEM image of a fully processed tip is shown in Fig. 3.

The rear contact of the probe is realized with a 250 μm platinum wire, which is simply stuck into the rear opening of the pipette and jammed into the taper of the capillary. This thicker wire thus makes mechanical contact with the inner wire without further fixation, avoiding to use other conducting materials which could cause unwanted parasitic thermocouples.

IV. ELECTRICAL AND THERMAL CHARACTERIZATION OF THE PROBE

The thermal properties of the probe are specified by its thermal resistance and its thermal capacity. In principle, a high thermal resistance is desirable in order to obtain a large thermovoltage signal. Since the total thermal conductivity of the probe results from both the metallic parts and the glass capillary, these components require individual treatment.

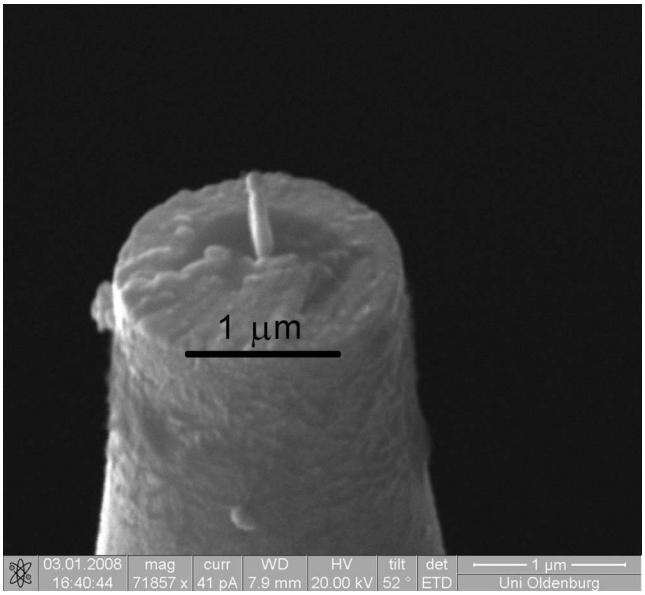

FIG. 3. SEM image of a thermocouple after having been processed in the micropipette puller as described in the text. The resulting glass/wire system has been covered with a 20-nm-thick gold film.

A. Electrical and thermal resistance of the metallic parts

The thermal resistance $R_{\mathrm{met}}^{\mathrm{th}}$ of the probe's metallic constituents is linked to their electrical resistance R^{el} through the Wiedemann–Fanz law,[19]

$$R_{\mathrm{met}}^{\mathrm{th}} = \frac{3}{T}\left(\frac{e}{\pi k_{\mathrm{B}}}\right)^2 R^{\mathrm{el}}, \tag{5}$$

where e denotes the charge of an electron and k_{B} is Boltzmann's constant.

Since the validity of the Wiedemann–Franz law has been confirmed for aluminum films with a thickness even down to 20 nm,[20] and the electrical conductivity of aluminum is similar to that of gold (Al: 35×10^6 S/m; Au: 43.5×10^6 S/m), it appears reasonable to assume that the Wiedemann–Franz law indeed applies to the metallic components of the miniature probes.

The electrical resistance of the gold film and the platinum wire are obtained individually by measuring the voltage drop induced by a tunneling current flowing over the respective leg of the thermocouple; for these measurements one leg is connected to ground and the other serves as a lead to contact the probe. The induced signal is superimposed on the thermovoltage, so that measurement of the film or wire resistance can only be made by registering the change in voltage caused by a change in the tunneling current. Data obtained in this manner are collected in Fig. 4; typical values of film resistances $R_{\mathrm{Au}}^{\mathrm{el}}$ are in the range of 100–500 Ω; typical values for the resistance of the wire $R_{\mathrm{Pt}}^{\mathrm{el}}$ are in the range of 10–50 Ω. The resistance of the film thus exceeds that of the wire.

The Wiedemann–Franz law [Eq. (5)] is used to calculate the thermal resistance of the metallic parts, which leads at the temperature $T=290$ K for the ranges of the electrical resistances given above to thermal resistances of the gold film $R_{\mathrm{Au}}^{\mathrm{th}}$ of $(1.4–7.0)\times10^7$ K/W and of the platinum wire

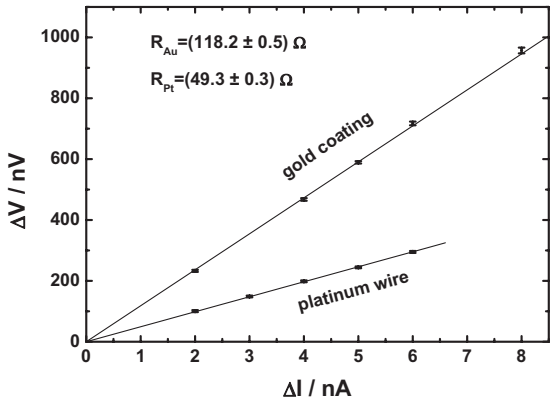

FIG. 4. Determination of the electrical resistance of the gold film R_{Au} and the platinum wire R_{Pt} by measuring the change in voltage ΔU caused by a change in the tunneling current ΔI.

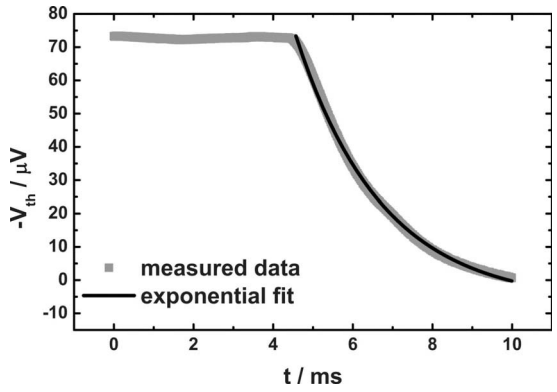

FIG. 6. Relaxation of the inverted thermovoltage signal after suddenly retracting the tip from tunneling distance. The signal decays with a characteristic time of 2.17 ms. The high initial level of the signal is caused by directly coupling the tip to the sample surface through a small particle.

$R_{\mathrm{Pt}}^{\mathrm{th}}$ of $(1.4-7.0)\times 10^6$ K/W. Concerning the heat current the two metals are connected in parallel and the smaller resistance $R_{\mathrm{Pt}}^{\mathrm{th}}$ determines the contribution of the metallic components to the thermal resistance of the probe.

B. Thermal resistance of the glass

Despite the fact that glass has a much higher thermal resistivity than metals, the glass capillary contributes significantly to the heat conduction of the probe, since its cross sectional area is large compared to those of the gold film and the platinum wire. The thermal resistance $R_{\mathrm{glass}}^{\mathrm{th}}$ of a capillary can be estimated by deducing the cross sectional areas of the glass from a microscope image, as exemplified in Fig. 5. For the probe depicted there, the thermal resistance of 1.3 mm length of glass body adjacent to the tip amounts to 2.1×10^6 K/W, with the foremost 34 μm contributing half in that value. The part not captured by the microscope image has such a large cross sectional area that it contributes less than 5% of the total resistance. Thus the thermal resistance of the metallic components and that of the capillary are in the same range and their connection in parallel leads to a total thermal resistance of the probe $R_{\mathrm{Pr}}^{\mathrm{th}}$ on the order of 1×10^6 K/W.

A reduction in the thickness of the gold film would not at all lead to a higher thermal resistance and a thinner platinum wire would not increase this resistance considerably. Such reductions would, in fact, be counterproductive, since they would increase the electrical resistance R^{el} only, and thereby increase the Johnson noise.

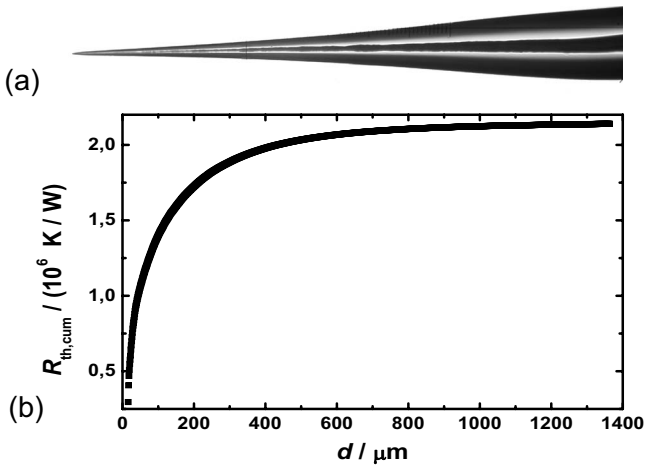

FIG. 5. (a) Microscope image of the foremost 1.3 mm of a thermocouple tip. From such pictures, the cross sectional areas of the glass are determined, taking into account the apparent magnification of the wire by the glass. (b) Cumulative thermal resistance $R_{\mathrm{th,cum}}$ of the glas from the tip to a position along the shaft. Observe that the foremost 34 μm contribute half of the total resistance.

C. Response time of the probe

The response time of a thermocouple is determined by both its thermal resistance and its thermal capacity. It is measured by suddenly retracting the tip from tunneling distance to a position 500 nm away from the surface, where no heat transfer is detectable. As shown in Fig. 6, the signal then decays with a time constant $\tau=2.17$ ms, corresponding to a bandwidth of about 460 Hz. The 2.17 ms are determined by the amplifier bandwidth and therefore the actual response time of the tip is shorter. Even though the response time of the thermovoltage signal allows sampling frequencies higher than 500 Hz, the measurements are carried out with a bandwidth Δf of 30 Hz only, in order to suppress the effects of voltage toggling in the preamplifier (290 Hz), and the noise caused by the power lines (50 Hz).

D. Seebeck coefficient of the probe

The Seebeck coefficient S links the thermovoltage produced by a thermocouple to the temperature difference ΔT_{sig} between its two ends, according to Eq. (3). It is a characteristic property of the two metals involved, in our case platinum and gold. Hence, we determine this coefficient as an average over a set of probes. To do so, the probes are dipped into a droplet of oil in a heating coil. The oil's temperature is varied between 20 and 90 °C, and measured with a commercial thermocouple. The corresponding signals provided by the probes are plotted versus temperature, and the temperature-dependent Seebeck coefficient is determined from the slope of the resulting curve, as illustrated in Fig. 7. In accordance with the data reported in Ref. 21 we obtain an approximately linear increase in the Seebeck coefficient with

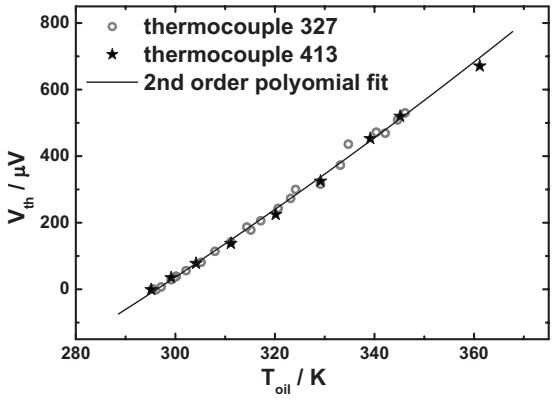

FIG. 7. Thermovoltage delivered by a probe when its tip is dipped into a heated droplet of oil, the temperature of which is monitored by a commercial thermocouple. The temperature-dependent Seebeck coefficient is determined from a second-order fit to the data.

temperature, resulting in a value for S of 9.5 μV/K at ambient temperature. This value exceeds the tabulated reference data[21] by about 3 μV/K, possibly due to an unwanted additional thermocouple, or nanoscale effects.

V. PERFORMANCE OF THE INSTRUMENT

When operated in ordinary STM mode, the position of the probe can be determined precisely both in a horizontal plane parallel to the sample's surface and with respect to the distance from that surface. The NSThM mode then allows one to monitor the distance dependence of the near-field heat transfer at a well-defined particular spot, and to obtain a thermal image of the sample surface.

A. STM functionality

The functionality of the instrument as a STM is demonstrated by examining a flat gold surface on mica, prepared by electron-beam evaporation of gold on heated mica.[22] In addition, gold nanoparticles have been deposited on this surface by dip coating. A STM topography is shown in Fig. 8; several gold layers separated by monatomic steps can be clearly identified. The measured step height amounts to (217 ± 26) pm, which is in agreement with the value of 236 pm expected for the height of monatomic steps on Au(111) surfaces. The present instrument, thus is capable of atomic resolution in the vertical direction.

B. Thermovoltage measurement and *z* spectroscopy

The thermovoltages generated by the thermocouple are amplified and low-pass filtered (30 Hz) by a commercial preamplifier/multimeter system (Keithley 1801/2001) and an amplifier (Stanford SR560). Finally they are tuned with a homemade amplifier to the input range of the control unit of the STM, into which they are fed in order to synchronize them with the position data. The measurement noise is determined from acquiring thermovoltage data with the tip in tunneling contact with the sample, and analyzing the distribution of the registered signals. This gives a value for the thermovoltage noise of $2\ \mathrm{nV}/\sqrt{\mathrm{Hz}}$ equivalent to a temperature noise of $0.2\ \mathrm{mK}/\sqrt{\mathrm{Hz}}$ (with $S=10\ \mu\mathrm{V/K}$). The thermovoltage signal is independent of the voltages applied to the piezos, as can be deduced from scans carried out when tip and samples are at ambient temperature. There is no detectable correlation between the topographical STM image and the thermovoltage image, as long as the tunneling current can be kept constant by the feedback loop. There exists an influence of the tunneling current on the thermovoltage, because it is running through the gold leg of the thermocouple. Over a resistance of a gold leg of 100 Ω, a typical tunneling current of 1 nA causes a voltage drop of 0.1 μV, which amounts to some percent of the thermovoltage signal in tunneling distance. Undisturbed data can therefore only be acquired when there is no tunneling current, i.e., when the gap voltage is switched off or the distance between the sample and the tip exceeds 3 nm, so that the tunneling current has ceased. Tunneling current artifacts showing up in the thermovoltage images can be accounted for by subtracting the voltage drop due to the tunneling current, using the known resistance of the gold leg.

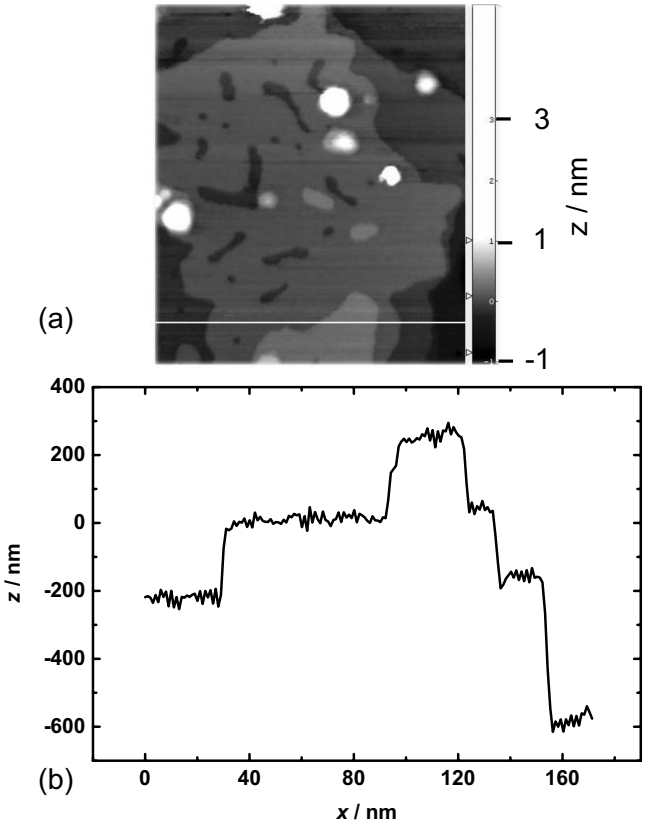

FIG. 8. (a) STM image and (b) scan along the line indicated in (a) of a gold surface, as recorded with the thermocouple probe acting as STM tip. The step height determined from (b) is close to the expected value for a Au(111) surface. The white spots visible in (a) result from deposited nanoparticles.

The dependence of the thermovoltage on the vertical distance z of the probe from the sample is determined from a series of measurements, termed z spectroscopy, such that each data point represents an average over 200 ms after a relaxation time of 1.8 s. Since the relaxation time of the probe is shorter than 2.17 ms, and the amplifier chain is operated at a bandwidth of 30 Hz, this waiting time ensures that all data are acquired in a thermodynamically steady state. The signal falls below the detection limit at a distance

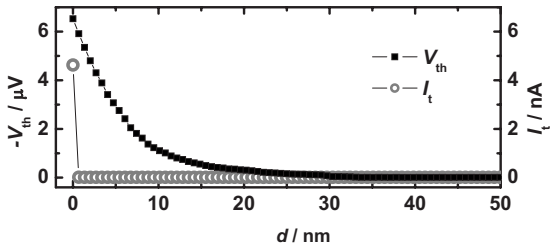

FIG. 9. Distance dependence of the inverted thermovoltage (left ordinate) and the tunneling current (right ordinate). Observe that a thermovoltage signal is detectable at distances an order of magnitude larger than those yielding a sizeable tunneling current.

of about 30 nm, as shown in Fig. 9. This finding clearly demonstrates that the interaction range of the thermal near-field radiation extends much farther than the tunneling distance. However, the detection limit of our setup is hit at distances much smaller than the wavelength of a blackbody emitter at ambient temperature, corresponding to 10 μm.

C. Near-field thermal imaging

For demonstrating the instrument's capability of thermal imaging, we scan cooled gold surfaces in constant tunneling current mode, that is, the probe-sample distance z is continuously adjusted such that the tunneling current remains constant, while the thermovoltage signal is recorded simultaneously. One then obtains thermovoltage images showing a strong contrast. As in the example depicted in Fig. 10, such thermographic NSThM images are anticorrelated with the corresponding topographic STM images. Since there is no thermovoltage signal when the sample is scanned at room temperature, and the thermovoltage shows a z dependence which is quite different from that of the tunneling current, this finding is a genuine feature. The similarity of the topographic and the thermographic picture is likely to be a "ridge-and-valley" effect: the electronic wave function determining the tunneling current has a range much shorter than that of the thermal evanescent near field. When the probe dips into a valley while maintaining a fixed value of the tunneling current, the heat current is higher than above flat pieces of the surface because the walls act as additional sources for the longer-ranged heat transfer via evanescent fields.

A detailed discussion of characteristic thermographic signatures provided by particular sample structures is deferred to a future study. In particular, it is of interest to investigate thermally active devices, for which there is no simple correlation between the topographic and the thermographic image. As an appealing option, such studies can also be performed in constant heat flow mode, replacing the constant tunneling current mode which necessarily emphasizes topography. It deserves to be pointed out already here that, in principle, a thermographic image can reveal structures with a linear size of a few nanometers, as witnessed by Fig. 10.

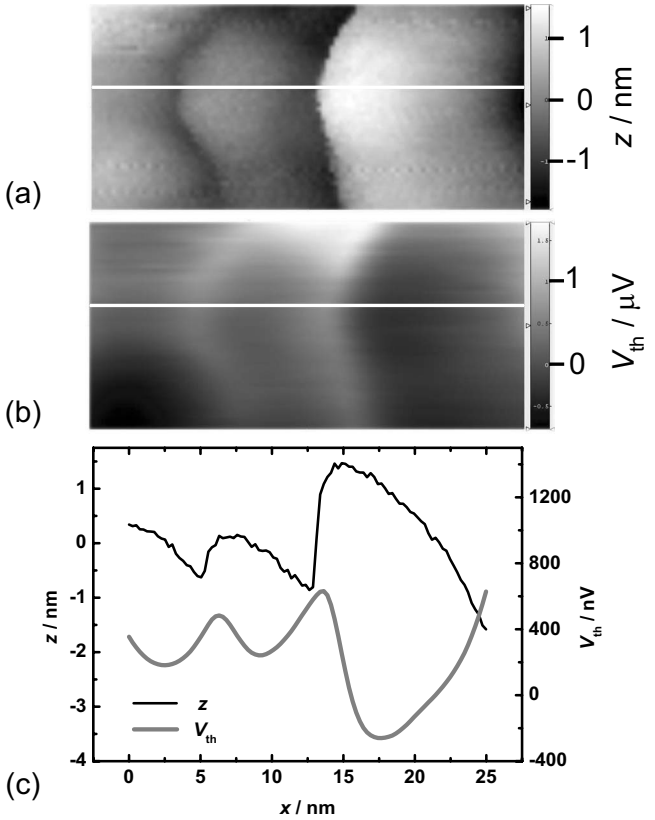

FIG. 10. (a) STM topography and (b) NSThM (rel V_{th}) thermography of a 12×25 nm^2 cooled gold surface, obtained in constant tunneling current mode. The line scan (c) has been made along the white line indicated in (a) and (b). A low thermovoltage signal corresponds to a lower temperature of the tip and thus to an increased heat transfer between probe and sample. Observe that here the thermovoltage image approximately is the inverted STM image, with a spatial resolution on the order of a few nanometers.

VI. CONCLUSION

The NSThM discussed in this paper provides far reaching new possibilities for experimental studies of thermal near-field effects. It is able to provide both detailed thermographic images of sample surfaces, and thermal z spectroscopies for vertical probe-sample distances ranging from 1 to some 10 nm.

Typical thermovoltage signals V^{th} in tunneling distance are about 5 μV. The instrument thus registers according to Eq. (4) with a Seebeck coefficient S of the probe of about 10 μV/K and an estimated thermal resistance R_{Pr}^{th} on the order of 10^6 K/W a heat current $\dot{Q}$ of about 5×10^{-7} W.

This instrument is thus capable of measuring the heat transfer by evanescent fields in the direct vicinity of the sample, which could not be achieved by the experiment in Ref. 10. Whereas our measurements are carried out in tunneling distance and the signal vanishes in the noise for distances larger than some 10 nm, the mean distance of the measurements in Ref. 10 was about 150 nm. Therefore the experiments were performed in different distance domains which might explain the different findings. Furthermore the geometries of the experiments are different: Xu *et al.*[10] realized two half spaces facing each other whereas our experiment is better described by a sphere or a cone opposing a half space.

The perspectives opened up by these developments concern at least two different issues. On the one hand, thermal near-field imaging of thermally active devices, even without the need of an absolute determination of the heat current,

may provide important new insights for nanoscale thermal engineering. On the other hand, the possibility to measure the near-field heat current absolutely allows one to make contact with theoretical predictions made by fluctuating electrodynamics,[2,5] and to perform experimental tests even at distances where this macroscopic theory might no longer be fully applicable. To this end, a more precise calibration of the instrument especially of its thermal resistance is desirable. We will take up these lines of investigation in subsequent publications.

ACKNOWLEDGMENTS

The authors would like to thank Martin Holthaus, Svend-Age Biehs, Oliver Huth, Felix Rüting, and Jürgen Parisi for the fruitful discussions. This work was supported in part by the Deutsche Forschungsgemeinschaft through Grant No. KI 438/8-1.

[1] A. Majumdar, Annu. Rev. Mater. Sci. **29**, 505 (1999).
[2] S. M. Rytov, *Theory of Electrical Fluctuations and Thermal Radiation* (Academy of Sciences Press, Moscow, 1953) (English translation by H. Erkuu, Air Force Cambridge Research Center, Bedford, MA, 1959).
[3] S. M. Rytov, Y. A. Kravtsov, and V. I. Tatarskii, *Principles of Statistical Radiophysics* (Springer, New York, 1989), Vol. 3.
[4] C. M. Hargreaves, Phys. Lett. **30A**, 491 (1969).
[5] D. Polder and M. Van Hove, Phys. Rev. B **4**, 3303 (1971).
[6] G. Binnig, H. Rohrer, Ch. Gerber, and E. Weibel, Phys. Rev. Lett. **49**, 57 (1982).
[7] G. Binnig, C. F. Quate, and Ch. Gerber, Phys. Rev. Lett. **56**, 930 (1986).
[8] C. C. Williams and H. K. Wickramasinghe, Appl. Phys. Lett. **49**, 1587 (1986).
[9] J. B. Xu, K. Läuger, K. Dransfeld, and I. H. Wilson, Rev. Sci. Instrum. **65**, 2262 (1994).
[10] J.-B. Xu, K. Läuger, R. Möller, K. Dransfeld, and I. H. Wilson, J. Appl. Phys. **76**, 7209 (1994).
[11] W. Müller-Hirsch, A. Kraft, M. T. Hirsch, J. Parisi, and A. Kittel, J. Vac. Sci. Technol. A **17**, 1205 (1999).
[12] A. Kittel, W. Müller-Hirsch, J. Parisi, S.-A. Biehs, D. Reddig, and M. Holthaus, Phys. Rev. Lett. **95**, 224301 (2005).
[13] Y. De Wilde, F. Formanek, R. Carminati, B. Gralak, P.-A. Lemoine, K. Joulain, J.-P. Mulet, Y. Chen, and J.-J. Greffet, Nature (London) **444**, 740 (2006).
[14] M. Stopka, L. Hadjiiski, E. Oesterschulze, and R. Kassing, J. Vac. Sci. Technol. B **13**, 2153 (1995).
[15] E. Oesterschulze, M. Stopka, L. Ackermann, W. Scholz, and S. Werner, J. Vac. Sci. Technol. B **14**, 832 (1996).
[16] K. Luo, Z. Shi, J. Varesi, and A. Majumdar, J. Vac. Sci. Technol. B **15**, 349 (1997).
[17] I. W. Rangelow, T. Gotszalk, N. Abedinov, P. Grabiec, and K. Edinger, Microelectron. Eng. **57**, 737 (2001).
[18] G. Fish, O. Bouevitch, S. Kokotov, K. Lieberman, D. Palanker, I. Turovets, and A. Lewis, Rev. Sci. Instrum. **66**, 3300 (1995).
[19] N. W. Ashcroft and N. D. Mermin, *Solid State Physics* (Harcourt College, Fort Worth, 1976).
[20] T. Stärz, U. Schmidt, and F. Völklein, Sens. Mater. **7**, 395 (1995).
[21] M. Gotoh, K. D. Hill, and E. G. Murdock, Rev. Sci. Instrum. **62**, 2778 (1991).
[22] N. Vandamme, E. Janssens, F. Vanhoutte, P. Lievens, and C. Van Haesendonck, J. Phys.: Condens. Matter **15**, 2983 (2003).